Hearing in Australian sea lions

Theme: Noise

WAMSI Westport Marine Science Program

WESTERN AUSTRALIAN MARINE SCIENCE INSTITUTION

WESTPORT

Better science **Better decisions**

WAMSI WESTPORT MARINE SCIENCE PROGRAM

WESTERN AUSTRALIAN MARINE SCIENCE INSTITUTION

WESTPORT

ABOUT THE MARINE SCIENCE PROGRAM

The WAMSI Westport Marine Science Program (WWMSP) is a $13.5 million body of marine research funded by the WA Government. The aims of the WWMSP are to increase knowledge of Cockburn Sound in areas that will inform the environmental impact assessment of the proposed Westport development and help to manage this important and heavily used marine area into the future. Westport is the State Government's program to move container trade from Fremantle to Kwinana, and includes a new container port and associated freight, road and rail, and logistics. The WWMSP comprises more than 30 research projects in the biological, physical and social sciences that are focused on the Cockburn Sound area. They are being delivered by more than 100 scientists from the WAMSI partnership and other organisations.

FUNDING SOURCES
The $13.5 million WAMSI Westport Marine Science Program was funded by the Western Australian Government, Department of Transport. WAMSI partners provided significant in-kind funding to the program to increase the value to >$22 million.

DATA
Finalised datasets will be released as open data, and data and/or metadata will be discoverable through Data WA and the Shared Land Information Platform (SLIP).

YEAR OF PUBLICATION
July 2024

This report is part of the project:: Hearing sensitivity of Australian sea lions, little penguins and fish

CITATION
Wei, C., Erbe, C. (2024). Hearing in Australian sea lions. Prepared for the WAMSI Westport Marine Science Program. Western Australian Marine Science Institution, Perth, Western Australia. 28 pp.

FRONT COVER IMAGE
Theme: Noise

Contents

The WAMSI Westport Marine Science Program is a $13.5 million body of research that is designed to fill knowledge gaps relating to the Cockburn Sound region. It was developed with the objectives of improving the capacity to avoid, mitigate and offset environmental impacts of the proposed Westport container port development and increase the WA Government's ability to manage other pressures acting on Cockburn Sound into the future. Funding for the program has been provided by Westport (through the Department of Transport) and the science projects are being delivered by the Western Australian Marine Science Institution.

1 Title: Hearing in Australian Sea Lions

Author/s
Chong Wei, Centre for Marine Science and Technology, Curtin University; chong.wei@curtin.edu.au
Christine Erbe, Centre for Marine Science and Technology, Curtin University; c.erbe@curtin.edu.au

Project
Curtin Project Number: RES 64483
CMST Project Number: 1594-4

Date
15 February 2024

Executive Summary

In the absence of noise exposure guidelines to inform marine environmental impact assessment (EIA), the first step in understanding the potential impacts and in designing noise reduction and mitigation methods is understanding whether the animals are sensitive to the noise sources from marine construction and operations. Knowledge of these animals' hearing sensitivity (e.g., what these animals can hear, how well they can hear, etc.) is important to understanding how these animals, many of which are endangered, may be affected by anthropogenic noise. An audiogram (i.e., curve of hearing sensitivity as a function of acoustic frequency) is the fundamental information for understanding hearing and for assessing noise impacts. However, this information is still unknown for the Australian sea lion, the main marine mammal species occurring in the Cockburn Sound region. This is due to the fact that Australian sea lions are not found in laboratories and rarely in aquaria and thus are inaccessible for training for live, behavioural experiments. Therefore, we still do not know what they can hear and how well they can hear, making it difficult to assess potential noise impacts and to design mitigation methods for this endangered species.

To fill this gap, our research collected a deceased Australian sea lion for computed tomography scans. The complex head structures, particularly the hearing structures (ear canals, inner ears, middle ears, tympanic bone) were reconstructed in detail based on high-resolution imaging data, and 3D digital models were built to simulate the processes of how the animal hear sounds in air and under water.

To study the sound reception mechanisms, the received sound pressure and displacement fields of the hearing-related structures were computed. The synergistic response of ear components to incident in-air and underwater sounds at selected frequencies was also calculated. Additionally, our models calculated two frequency-dependent transfer functions (in air and under water) between the magnitude of the velocity at the stapes footplate and the amplitude of input sound pressure. The transfer functions were used to predict the in-air and underwater audiograms for the Australian sea lion.

In general, our predicted in-air and underwater audiograms showed good agreement with those of California sea lions in both the form and range of hearing sensitivity. However, audiogram curves slightly vary among individuals (e.g., with sex, age, and health) and among species (e.g., the general shape of the Steller sea lion aerial audiogram was similar to those of California sea lions and the Australian sea lion, but the hearing thresholds were higher across the entire frequency range). This is likely related to the morphology differences, such as the different head sizes, the anatomy differences of the head, etc. Therefore, collecting more Australian sea lion specimens for modelling is an important future work to capture variability in audiograms. Moreover, two caveats must be pointed out. First, due to safety and health concerns, the tissue properties of the specimen were not

measured in this research. Second, due to the limited computing power of our current computer, the in-air model only predicted the in-air audiogram from 100 Hz to 20 kHz and the underwater model only predicted the underwater audiogram from 100 Hz to 40 kHz. Performing tissue property measurement and upgrading the computer for wider frequency range modelling would be the logical follow-on to this research.

In summary, our research developed a promising method to derive the first in-air and underwater audiograms of the endangered Australian sea lion, males of which seasonally reside on islands in the Cockburn Sound area. The results suggest that the guidance for California sea lions from the previous study (Southall et al., 2019) can be applied as a reference in the EIA and management plans, for instance, distances for management (exclusion and observation) zones. The results provide a valuable indication of what frequency of sounds these animals can hear and how well they can hear. The outputs from this study can assist efforts in understanding the potential impacts, designing noise reduction methods, and devising mitigation plans for Australian sea lions.

2 Introduction

The Australian sea lion (ASL; *Neophoca cinerea*) is the only sea lion species endemic to Australia (occurring in South and Western Australia). The species is recognized as one of the world's most endangered pinnipeds (seals, sea lions, and walruses). The high level of past hunting coupled with high natal site fidelity (i.e., females needing to return to the same site, so limited movement across islands) has resulted in this species' small and genetically fragmented populations (Campbell et al., 2008). The number of ASLs has fallen by over 60% in four decades. The species is globally classified as "endangered" (IUCN Red List) (Goldsworthy, 2015). In 2021, the species was re-assessed and listed as "endangered" in Australia under the Environment Protection and Biodiversity Conservation Act (EPBC Act 1999) and Biodiversity Conservation Act 2016.

ASLs breed on offshore islands where pups congregate around rock or vegetation shelter while the mothers hunt and feed in offshore feeding grounds (Gales et al., 1994). Their breeding cycle (17-18 months) is unusual compared to that of other species within the pinniped family (12 months). Additionally, the strong site fidelity to their natal island along with asynchronous breeding between islands make each of the pupping grounds and their associated feeding grounds critical habitat (Gales et al., 1992). According to the Recovery Plan from the Department of Climate Change, Energy, the Environment and Water (DCCEEW), 58 breeding sites are considered habitat critical to the survival of the species.

ASLs and their habitats are under threat (DCCEEW, 2013). Since the industrialization of the oceans, steadily increasing marine noise has become a worldwide issue. The volume and spatial extent of marine noise pollution have become one of the significant threats to marine animals. For example, previous studies have shown that seals are known to display strong avoidance behaviour (swimming rapidly away from the source) and cessation of feeding in response to seismic surveys (Thompson et al., 1998). Similar avoidance responses were documented during trials with grey seals: They changed from making foraging dives and moving away from the source, and some seals hauled out, possibly to avoid the noise (Aarts et al., 2018). Therefore, the Australian Government (DCCEEW) acknowledges that pinnipeds, including ASLs, are likely to be susceptible to noise levels or increased noise pollution from various noise sources, such as seismic surveys, construction activities, shipping, etc. (Gordon et al., 2003). Unfortunately, the lack of important information regarding ASL sound reception mechanisms and their hearing sensitivity to various acoustic frequencies impedes the assessment of the impacts of anthropogenic noise on these animals (Southall et al., 2019).

An audiogram (curve of hearing sensitivity) is the auditory hearing threshold as a function of frequency, which is important information for assessing the potential noise impact on the animals and develop appropriate management or mitigation measures. Most of our knowledge of sea lion hearing sensitivity and hearing impairment stems from California sea lions (*Zalophus californianus*) in the USA. This species is the best-studied species among the Otariidae in terms of hearing in air and under water. Both in-air and underwater audiograms of this species have been tested on individuals of various ages and sexes using behavioural methods since the 1970s (Schusterman et al., 1972; Schusterman, 1974; Moore and Schusterman, 1987; Kastak and Schusterman, 1998; Mulsow et al., 2011; 2012; Reichmuth and Southall, 2012; Reichmuth et al., 2013; Reichmuth et al., 2017; Kastelein et al., 2023). The hearing sensitivity in the Steller sea lion (*Eumetopias jubatus*) has also been studied using psychophysical and electrophysiological methods (Kastelein et al., 2005; Mulsow and Reichmuth, 2010; Mulsow et al., 2012). However, neither the auditory capabilities nor auditory thresholds have been studied to-date for ASL.

The conventional methods for estimating audiograms can be classified into three categories: (A) predict audiogram based on the characteristics of the vocalizations (i.e., what animals can hear matches what they can generate) (Clark, 1990; Matthews et al., 1999); (B) predict audiogram based on ear anatomy and compare to the functional morphology of ears in well-known closely related species (Ketten, 1994; 1997; 2000); and (C) measure audiogram through practical methods, such as

behavioural response experiments and electrophysiological testing (e.g., auditory brainstem response; ABR) (Larsen et al., 2020). For category A, recent work has documented the characteristics of the vocalization (barking calls) of ASLs (Gwilliam et al., 2008; Ahonen et al., 2014). It is generally expected that most animals hear well around the peak frequencies of their vocal sounds. However, peak spectra are often close but not coincident with best hearing sensitivities (Tubelli et al., 2018). Moreover, animal vocalizations typically do not cover the entire hearing range. For instance, the hearing sensitivity of the common bottlenose dolphin (*Tursiops truncatus*) is approximately 100 Hz to 160 kHz, while their communication sounds (e.g., whistles) are typically only in the range 1–24 kHz and echolocation clicks 30–120 kHz (Au, 1993). Therefore, using vocalization characteristics can only provide a very rough estimation of the animals' hearing capabilities. Category B can only predict the hearing capabilities if audiograms from anatomically and ecologically similar or related species exist. Both categories A and B are unable to provide enough information about the hearing thresholds. Category C is also not reliable or practical to extract audiograms for ASL, because this species is on the endangered species list, thus the species is not found in laboratories and rarely in aquaria and thus inaccessible for training for live, behavioural experiments.

To overcome the challenges, here we developed sound reception finite-element (FE) models based on high-resolution computed tomography (CT) imaging. The imaging-based FE modelling techniques allow us to predict audiograms and study sound reception mechanisms in ASL. The techniques have been used to study the middle ears of multiple species of terrestrial mammals (Koike et al., 2002; Gan et al., 2004; Homma et al., 2009; 2010; Wang and Gan; 2016; De Greef et al., 2017; Tubelli et al., 2012; 2018). They also have been used to study sound reception and noise impact on multiple marine species, such as fish (Wei et al., 2022), baleen whales (Tubelli et al., 2012; 2018; Cranford and Krysl, 2015), and toothed whales (Aroyan, 2001). The techniques have the advantage of studying the complex acoustic processes when sounds interact with animal biological structures, becoming a useful tool when traditional experimental methods are not available. Based on the audiograms (in air and under water), we would be able to assess potential acoustic impacts on ASL and make relevant plans for mitigating the negative effects of anthropogenic noise on this endangered species, which are critical for conservation efforts.

3 Materials and Methods

3.1 Specimen and CT Scan

3.1.1 Specimen

On 07 July 2022, the Department of Biodiversity, Conservation and Attractions (DBCA) informed us of an ASL that had died in the afternoon at Carnac Island. According to the DBCA marine rangers, the animal was alive in the morning around 9 am but it was found dead around 2 pm, therefore it was a fresh specimen. We collected the fresh specimen on 08 July 2022. The specimen was a male adult, it died due to a boat strike. A deep wound on the body punctured into the body cavity, which was most likely fatal; the head of the specimen was intact, as shown in Figure 1A. We removed the head and sent it to the Animalius veterinary hospital in Bayswater, Western Australia for medical CT scanning in the late afternoon of the same day.

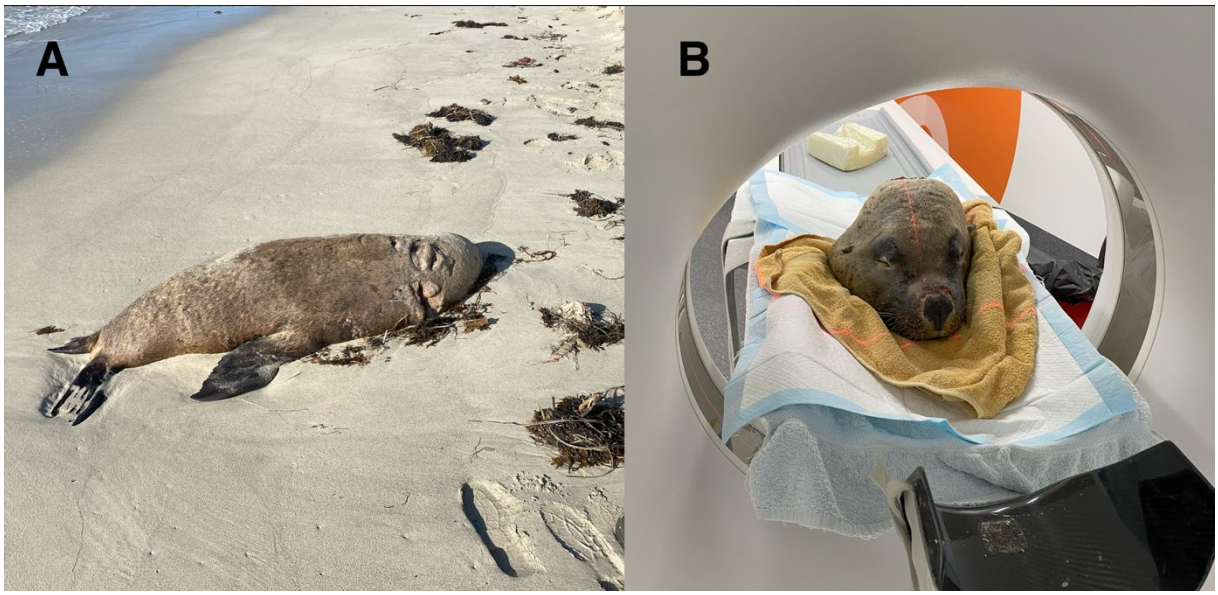

Figure 1. (A) A fresh dead ASL on Carnac Island. (B) Medical CT scan of the head of the ASL.

3.1.2 Medical CT Scan and Data Analysis

An accurate finite element hearing model requires high-accuracy inputs of geometric information and material properties. Medical CT scanning is a non-destructive technology that provides high-resolution 3D geometry information. It allows us to study the anatomy of the interior structures of animal specimens without having to cut the samples.

The specimen was scanned using a Siemens SOMATOM go. Up high-resolution scanner. The head was put on the scanner, as shown in Figure 1B. Images were acquired in the transaxial plane (i.e., at right angles to the long axis of the body) and helically by rotating an X-ray source of 130 kV at 300 mA. A total of 396 transverse slices of 0.8 mm thickness were collected, with a matrix size of 512 × 512. All the images were saved as DICOM files, which were later imported into the software Horos™ (Horos Project, Geneva, Switzerland) for CT data analysis and geometrical model reconstruction. The head was slightly deformed when it was scanned in the prone position due to gravity (see Figure 2A). Therefore, the 3D multiplanar reformation was performed to adjust the positions of the head in 3 views so the geometry would more closely represent that of an alive ASL. In the CT data analysis, the DICOM image stack of structures of interest was segmented, such as the soft tissues, skull, and ear apparatus (e.g., ear canals, inner ears, tympanic bone, etc.), as shown in Figures 2A-C. 3D reconstruction of the head was then conducted, with a length of ~330 mm, a height of ~215 mm, and a width of ~250 mm, as shown in Figure 2D. The Hounsfield Unit (HU) values of each structure in the animal's head were also derived. Each structure was exported as a stereolithography (STL) file after optimization and modification (e.g., smoothing, removing overlapping and self-intersections, etc.).

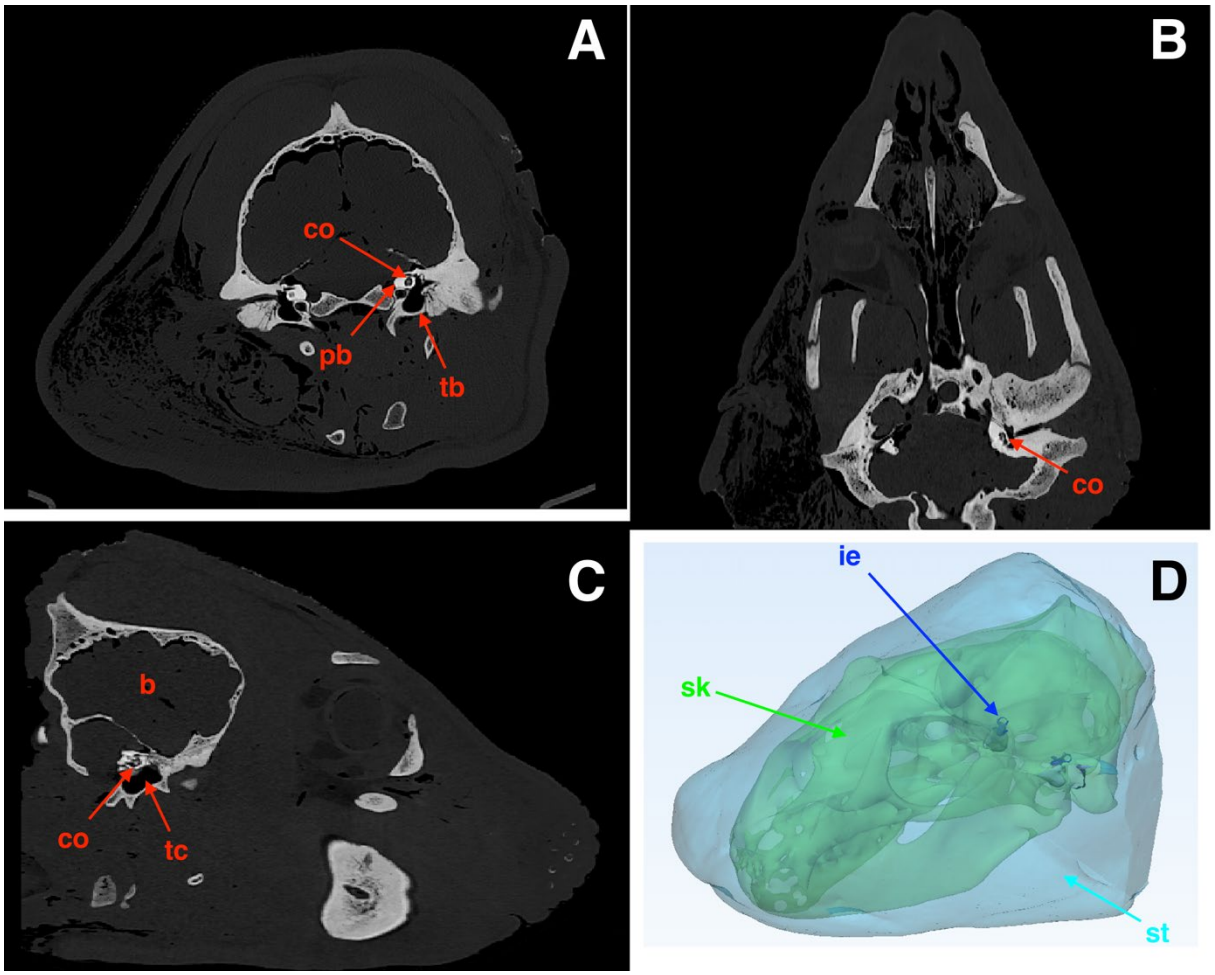

Figure 2. CT scan of an ASL head. (A) Cross plane, (B) frontal plane, and (C) sagittal plane of the head. The grey level represents the different HU values. (D) 3D reconstruction of the head and ear structures. More details can be found in the supplementary files. Abbreviations used in figures: co, cochlea; pb, periotic bone; tp, tympanic bone; b, brain; tc, tympanic cavity; ie, inner ear; sk, skull; st, soft tissue.

3.2 FE Modelling Techniques

Here we developed detailed, anatomically accurate sound reception FE models based on high-resolution CT data. The imaging-based FE modelling techniques allow us to predict audiograms and study sound reception mechanisms in ASL. Finite element analysis (FEA) is a numerical technique for finding approximate solutions to boundary-value problems for partial differential equations. The advantage of the FEA is the ability to deal with complex boundaries and to provide fine spatial information on the animal heads. The techniques have been used to study sound reception and hearing in several marine species, such as fish (Salas et al., 2019a, 2019b; Krysl et al., 2012; Wei et al., 2022), baleen whales (Cranford and Krysl, 2015; Tubelli et al., 2012; 2018), and toothed whales (Aroyan, 2001).

The STL files were imported into the COMSOL Multiphysics modelling software (Stockholm, Sweden) for FEA and corresponding data analysis. In this research we studied hearing in ASL in two scenarios: in-air (IA) hearing and underwater (UW) hearing. Therefore, two FE models were developed based on CT data: the IA model and the UW model. The models simulated the sound reception process from outside media (air or seawater) to the inner ear of an ASL. An air sphere and water sphere were set outside of the head for the IA and UW models, respectively, simulating an ASL receiving sound through air and seawater, as shown in Figure 3A. The diameter of the sphere was set as 400 mm.

A low-reflecting boundary condition (Bérenger, 1994) was applied to the sphere, simulating the sound transmitting in free space with minimum boundary reflections.

An incident acoustic wave was set in front of the left ear with a given pressure amplitude; the magnitude of the input pressure is arbitrary since the model is linear. The stimulus was directed toward the head at the selected frequencies, as the red arrow shown in Figure 3A. The frequency was swept from 100 Hz to 20 kHz in steps of 250 Hz for the IA model, whereas the frequency was swept from 100 Hz to 40 kHz in steps of 200 Hz for the UW model. The sound wave travelled through the air or sea water surrounding the sea lion's head and then interacted with the complex head structures to generate traction loads on the surface of the ears.

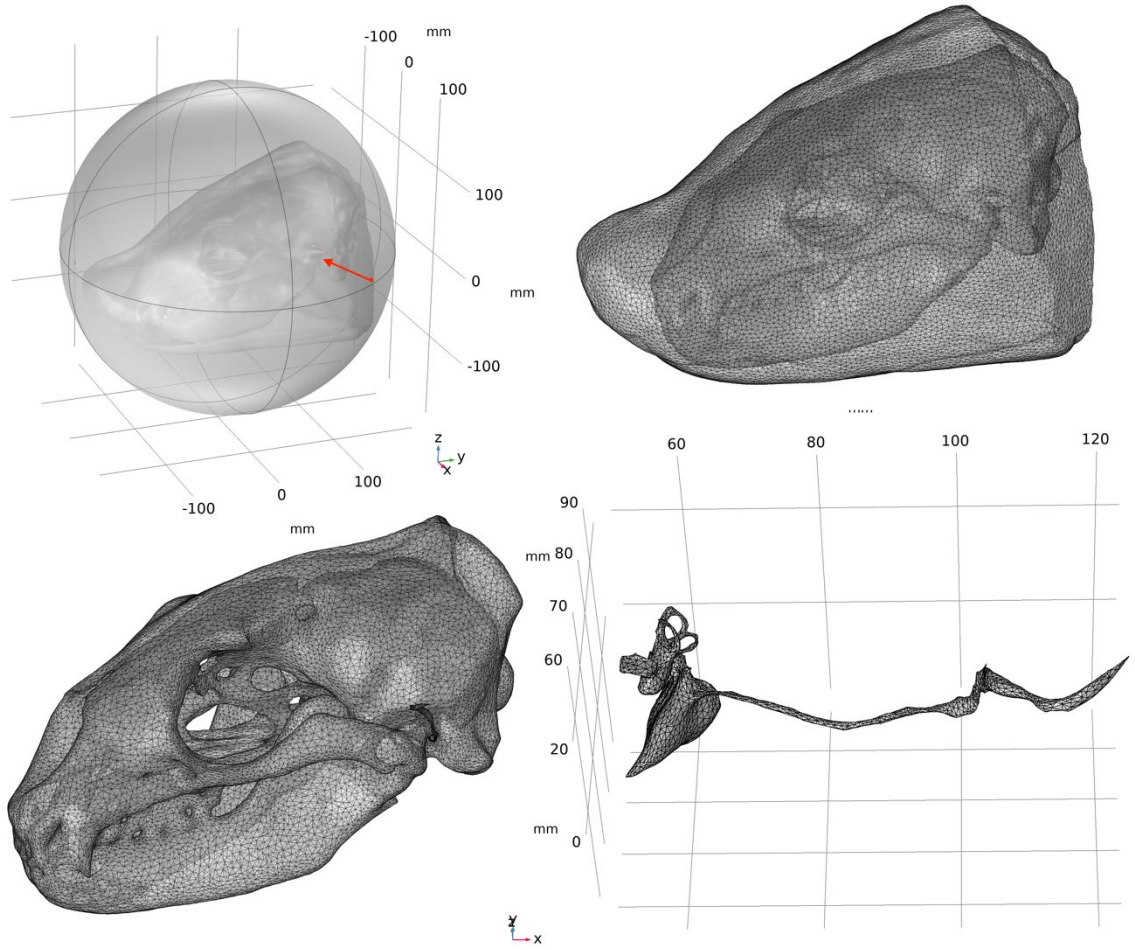

Figure 3. ASL FE hearing model. (A) The setup of the model based on CT data. The red point represents the acoustic stimulus and the red arrow shows the direction of the incoming sound. (B) The meshing of the ASL's head. (C) The meshing of the skull structure and ear structure. (D) The mesh of the inner ear (ie), tympanic cavity (tc), and the ear canal (ec).

The COMSOL's free mesher was used to generate a free tetrahedral mesh to map the entire model. The free mesh has built-in detection for small features and narrow regions in a geometry. It also has automatic element size adjustment to small features, narrow regions, and curved boundaries. It is widely accepted that the element size in element-based acoustic computations should be related to the wavelength. Often, the element size is measured in a certain (fixed) number of elements per wavelength. For the 3D acoustic modelling, the rule of thumb for meshing wave problems is to apply at least five to six second-order mesh elements per local wavelength to resolve waves, including

resolving elastic waves in the solid (Thompson and Pinsky, 1994; Ihlenburg, 2006). In this study, the maximum mesh size was set at least one-sixth of the wavelength at each frequency for each material (i.e., air, water, soft tissue, skull, etc.). To gain confidence in the accuracy of the model, a mesh refinement analysis/mesh convergence study was performed by re-solving the model on progressively finer meshes to find the optimal element size for the model. Based on the mesh refinement results, the size of the element for air was set between 1 and 2 mm, the size of the element for seawater was set between 5 and 7.5 mm, the size of the element for the soft tissues was set between 5 and 7.5 mm, the size of the element for the bony structures was set between 10 and 17.5 mm, and the size of the element of the ear structures (i.e., ear canal, inner ear, stapes, etc.) was set between 1 and 2 mm. The meshing is shown in Figures 3B, C, and D. For the IA model, the geometry translated to a mesh consisting of 5.62 million tetrahedral elements, resulting in the number of degrees of freedom (DOF) solved of 8.73 million. For the UW model, the geometry translated to a mesh consisting of 1.93 million tetrahedral elements, resulting in the number of degrees of freedom solved of 3.82 million. The mesh quality is shown in Figure 4.

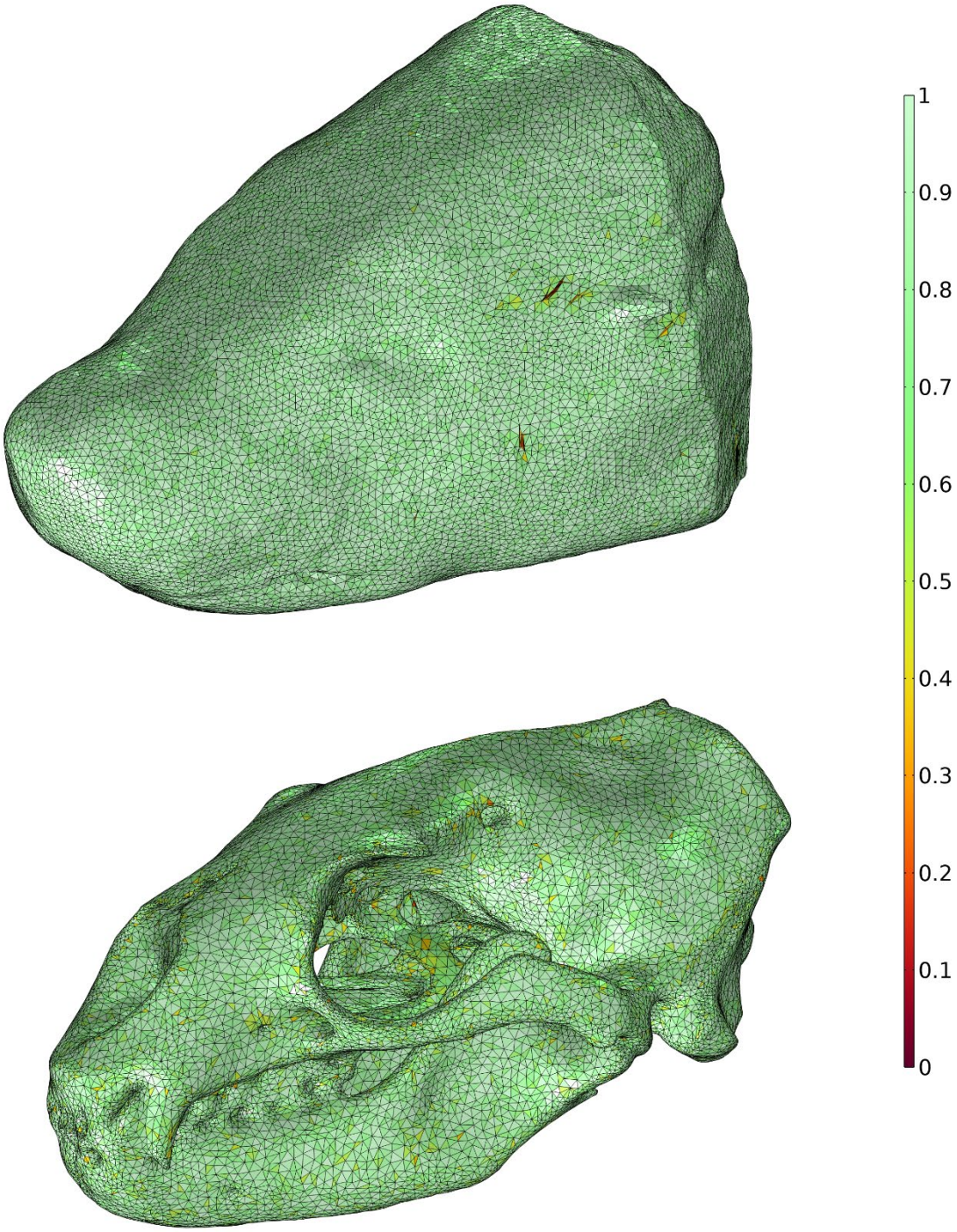

Figure 4. The mesh quality of the ASL models, including the full head (up) and skull (down). The color scale shows the quality of the mesh elements, from red (bad) to green (good). The mesh element quality is a dimensionless quantity between 0 and 1, where 1 represents a perfectly regular element, in the chosen quality measure, and 0 represents a degenerated element.

The finite-element Pressure Acoustics-Frequency Domain module coupled with Solid Mechanics and an Acoustic-Structure Boundary was applied for the models. When acoustic waves propagate within the liquid medium, the longitudinal waves can be written as:

$$\frac{1}{\rho_0 c_s^2}\frac{\partial^2 p}{\partial t^2} + \nabla \cdot \left(-\frac{1}{\rho_0}\nabla p\right) = 0 \quad (1)$$

where p is the sound pressure (Pa), ρ_0 is the density (kg/m^3), and c_s is the speed of sound (m/s). The density ρ_0 is included in the equation because of its variations in different computational domains within the model. For the harmonic solution of the pressure $p(\boldsymbol{x}, t) = p(\boldsymbol{x})e^{i\omega t}$, with the angular frequency ω (rad/s), Eq. 1 can be simplified as:

$$\nabla \cdot \left(-\frac{1}{\rho_0}\nabla p\right) - \frac{\omega^2 p}{\rho_0 c_s^2} = 0 \quad (2)$$

while the acoustic waves interact with the solid medium, the multiphysics coupling provides and assigns the boundary conditions for the two-way acoustic structural coupling between the liquid (e.g., water and soft tissues) and the solid (e.g., skull). The fluid-solid boundary condition includes the following interaction between fluid and solid domains:

$$\boldsymbol{F} = -\boldsymbol{n}_s p \quad (3)$$

$$-\boldsymbol{n}_a \cdot \left(-\frac{1}{\rho_0}\nabla p\right) = a_n \quad (4)$$

$$a_n = (\boldsymbol{n}_a \cdot \boldsymbol{u})\omega^2 \quad (5)$$

where $\boldsymbol{F}$ is the boundary load (force/unit area) on solid, $\boldsymbol{n}_s$ is the outward-pointing unit normal vector seen from inside the solid, p is the acoustic pressure, $\boldsymbol{n}_a$ is the outward-pointing unit normal vector seen from inside the liquid, ρ_0 is the density, a_n is normal acceleration of the solid surface in the liquid domain boundary, and $\boldsymbol{u}$ is the calculated harmonic displacement vector of the solid structure.

3.3 Reconstruction of Material Properties

According to the suggestion from the Curtin University Health & Safety Assessment team, conducting tissue properties measurement on the dead ASL potentially is of high risk because dead sea lions could carry diseases that can be transmitted to humans, such as tuberculosis. Therefore, in this study, we estimated physiologically relevant values for the tissue properties based on existing literature and knowledge of anatomical similarities. Previous studies have found linear relationships between the tissue acoustic properties (e.g., sound speed, density, and acoustic impedance) and HU values across different marine mammal species (Soldevilla et al., 2005; Wei et al., 2015). In the study of Wei et al. (2015), the HU-to-sound-speed and HU-to-density relationships were obtained based on the tissue measurement on a Yangtze finless porpoise (*Neophocaena asiaeorientalis*):

$$c = 1.1773 \times HU + 1501.4 \quad (6)$$

$$\rho = 0.0005 \times HU + 1.0008 \quad (7)$$

Since the mammalian tissue properties are conserved at the same temperature (Duck, 1990), we exported all HU values of each structure in the head of the ASL from the CT data, then converted all HU values to sound speed and density values using Eqs. 6 and 7. The acoustic property data was used to create 3D acoustic impedance models for FE models. This method has been used to construct FE models for a harbour porpoise and a bottlenose dolphin, respectively (Wei et al., 2017; 2018a). The FE modelling results of the two species matched direct measurements from live, echolocating animals, proving the reliability of this method (Wei et al., 2017; 2018a).

The values of material properties set for the models are shown in Table 1. The sound speed and density values can be derived by the HU values based on CT data. Young's modulus, the ratio of stress to strain that describes the stiffness of a material, was set from 30×10^3 to 60×10^3 MPa (Currey, 1979; Tubelli et al., 2012). Poisson's ratio, a ratio of transverse strain to longitudinal strain for bone, was set as 0.3 for the bony structures; this is a common value used for bone (Tubelli et al., 2014).

Table 1. Material property values for the ASL models.

Material	Sound Speed (m/s)	Density (kg/m^3)	Young's modulus (MPa)	Poisson's ratio
Sea water	1500	998		
Bony structures	3500–3800	2´10^3–2.3´10^3	30´10^3–60´10^3	0.3
Soft tissues	1320–1533	993–1400		
Inner ear	1466	1200		
Stapes	3500	2.3´10^3	35´10^3	0.3

3.4 Transfer Function

The ear (i.e., external, middle, and inner ear) can be seen as a series of components. The synergistic response of these ear components to incoming acoustic signals can together determine the audiogram (Tubelli et al., 2012; 2018; Cranford and Krysl, 2015). When the incident acoustic wave impinges upon the sea lion's head, it partially reflects off the skin and partially propagates further in the soft tissues (e.g., muscle). Some of the waves travel through the dense bony structures as elastic waves. The ears vibrate under the incident acoustic wave (p_{input}), resulting in the motion of the stapes within the oval window (the oval window is a connective tissue membrane located at the end of the middle ear and the beginning of the inner ear), which produces a velocity at the stapes footplate (v_{cf}), as shown in Figure 5. The motion in the ossicular chain causes the motion at the stapes footplate, which sits in the oval window of the cochlea. The motion of the stapes footplate pushing in and out of the oval window drives the fluid cochlea mechanically, causing the vibration on the inner ear.

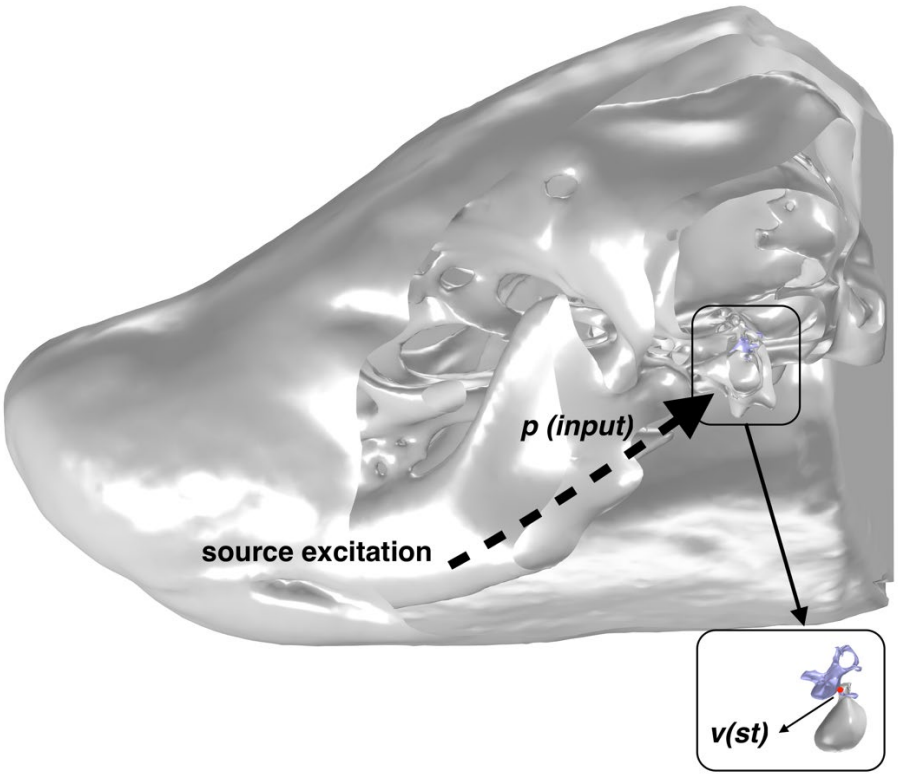

Figure 5. Schematic of the FE hearing model that extracts the cochlea input from the incident wave.

Based on this sound reception mechanism, an FE hearing model was performed using COMSOL Multiphysics (COMSOL Inc., Stockholm) to determine the frequency response of the hearing apparatus. The output of the model is a frequency-dependent transfer function (TF, p_{input} to v_{st}) between the magnitude of the velocity at the stapes footplate (v_{st}) and amplitude of input sound pressure (p_{input}), giving a TF with the units of nm/s/Pa. The modelling results were imported into OriginPro software (OriginLab, Northampton, MA, USA) for data analysis and plotting.

3.5 Audiogram Curve

The audiogram was predicted based on the TF results. The audiogram curve was calibrated with respect to the minimum audible pressure. This method has been used for other marine mammal species. For example, Cranford and Krysl (2015) assumed the hearing threshold of the fin whale to be similar to that measured for the bottlenose dolphin and killer whale (~70 dB re 1µPa). Here we assumed the hearing threshold of ASL to be similar to that of the California sea lion (0 dB re 20 µPa in air and 58 dB re 1µPa in water; Reichmuth et al., 2017; Kastelein et al., 2023; Southall et al., 2019). Then we estimated the minimum threshold pressure across all frequencies and computed the stapes velocity at the threshold through the peak value of the TF (Cranford and Krysl., 2015). OriginPro software was used to smooth the TF (adjacent-averaging method).

4 Results

Our FE models simulated the sound reception process of an ASL's head in air and under water. The sound pressure fields at each of the excitation frequencies were calculated. Figure 6 shows an example of the sound pressure field at 3 kHz exported from the UW model. The incident acoustic stimulus travelled through the water and was directly toward animal's head from the left side. The figure showed that relative sound pressure at the left ear was significantly higher than that at the right ear because the left ear was closer to the sound source excitation.

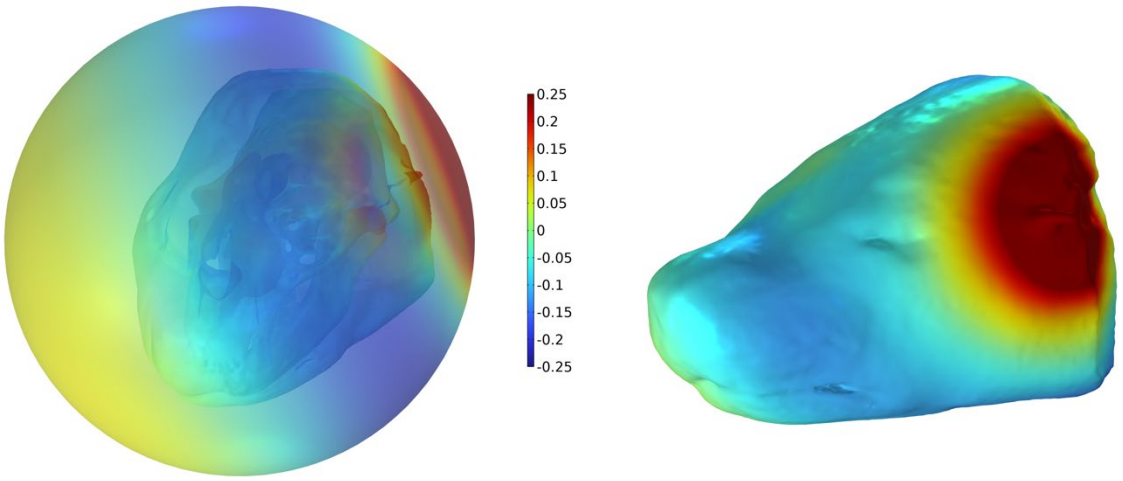

Figure 6. Sound pressure field of UW model at 3 kHz. The colour scale shows the relative amplitude of the sound pressure, which was normalized by dividing by the maximum values in the results.

In the sound reception process, the sound energy transmits from the outer ear (the outer ear of ASL is reduced and there is no external pinna) to the cochlea in the inner ear through a sound reception pathway. The inner ear converts the sound to electronic signals for the nerve cells. To further examine the inner ear response to the incident sounds (both in air and under water) during sound reception, the frequency responses of the inner ear (left) were computed here. Figure 7 shows an example of the left inner ear responses to the underwater stimulus.

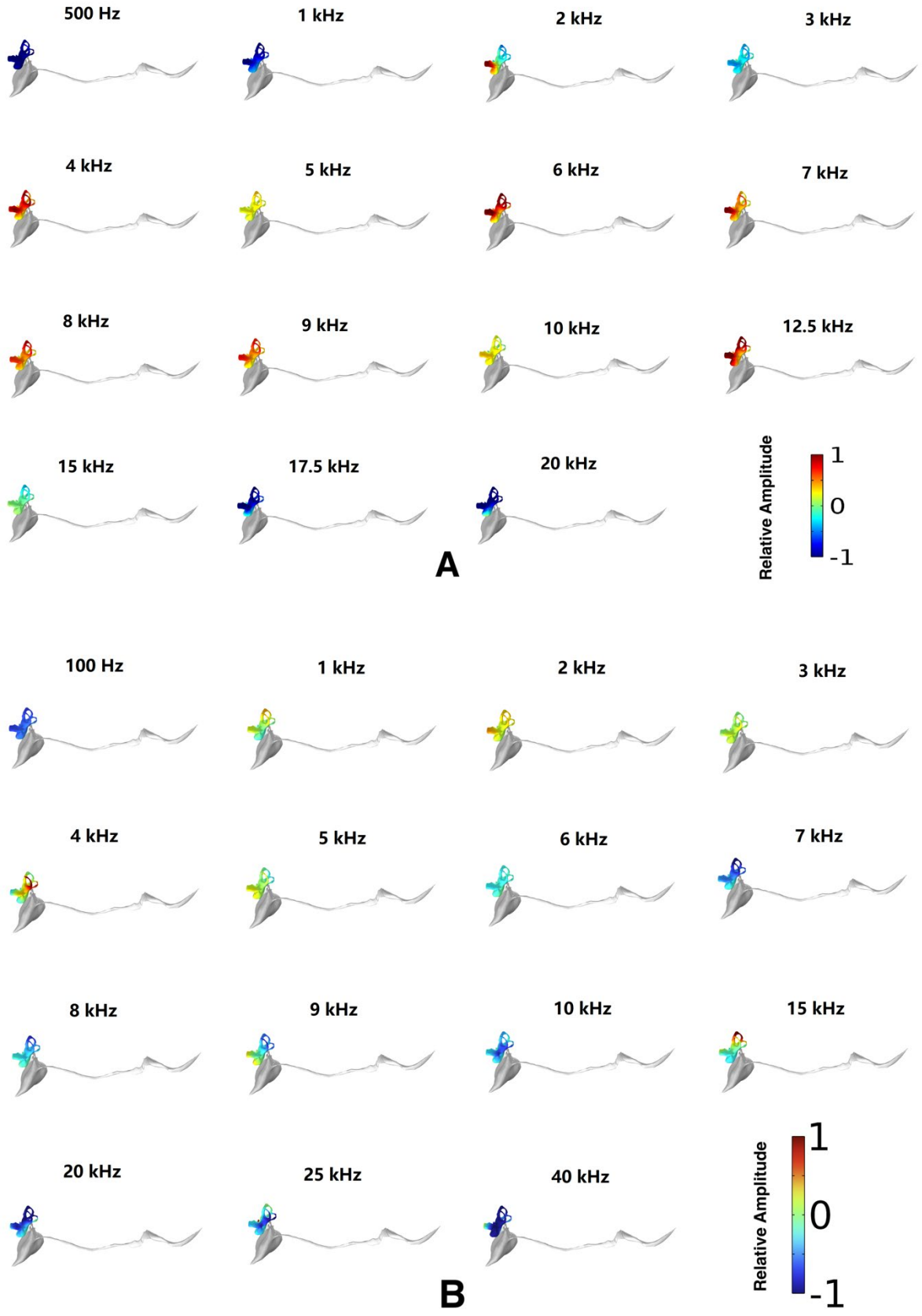

Figure 7. The response of the left inner ear to the aerial (A) and underwater (B) incident sounds in frequency ranges of 500 Hz–20 kHz and 100 Hz–40 kHz, respectively. The colour bars represent the relative amplitude of sound pressure. To focus on the sound pressure on the inner ear (especially the cochlea), the pressure on the ear canal (grey area) is not shown.

The cochlea in the left inner ear had better responses to the aerial sounds at frequencies from 4 kHz to 12.5 kHz. The relative amplitude of the sound pressure on the cochlea surface was significantly lower when the frequency was lower than 2 kHz and higher than 15 kHz. In the underwater scenario, the cochlea had the best responses to the underwater sounds at frequencies from 1 to 5 kHz. The relative amplitude of the sound pressure on the cochlea surface slightly dropped at frequencies from 6 to 15 kHz. The relative amplitude of the sound pressure at low frequency (100 Hz) and high frequency (> 20 kHz) was significantly lower than at the other frequencies.

The acoustic waves travelled through the animal's head and interacted with the complex head structures (i.e., muscles, fats, ear apparatus, skull, etc.), the elastic waves generated motion within the stiff and dense skull causing skull deformation. More details about skull deformation can be found in the supplementary files. The skull vibration created displacement. The displacement fields at each of the excitation frequencies were calculated. Figure 8 shows an example of displacement field exported from the UW model at 4 kHz.

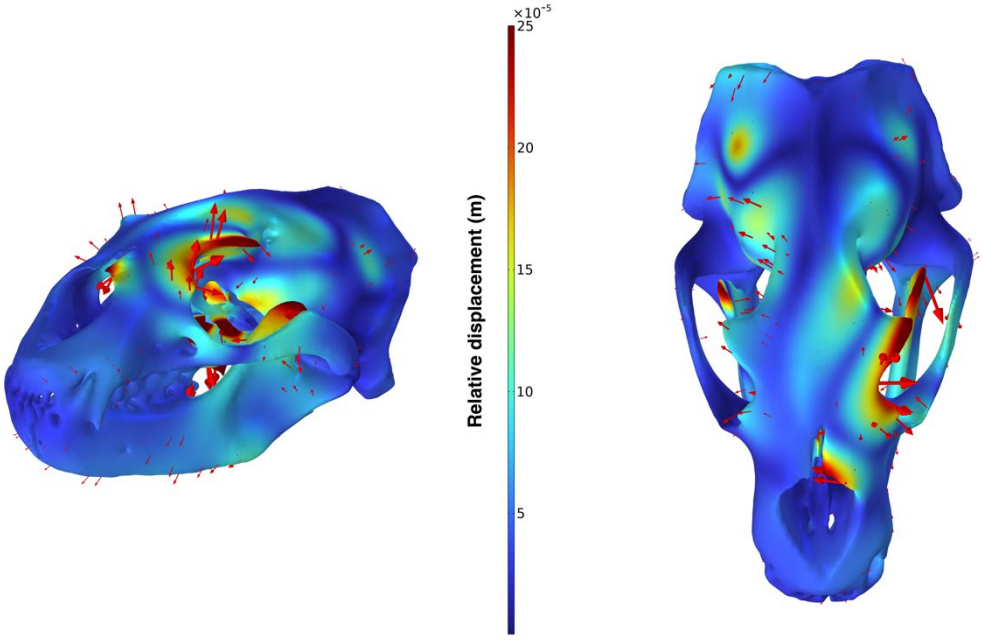

Figure 8. An example of the displacement field exported from the UW models at 4 kHz from two angles, the soft tissues are not shown here. The red arrows indicate both the direction and magnitude of the displacement. The colour bar indicates the relative magnitude of the displacement.

It is clear that the region close to the left ear had a higher magnitude of displacement. The motion was transmitted from the left side of the skull to the right side of the skull. In the cetacean ears, the periotic bones are firmly attached to the skull, whereas the tympanic bones do not attach to the skull directly (the tympanic and periotic bones are connected to each other through relatively flexible bony pedicles). When the incident sound creates vibrations in the skull, the skull vibrations are transmitted to the periotic bones directly, and the tympanic bones are forced to follow the vibrations. The tympanic bones are lagged behind the motions of the skull and periotic bones, creating differential motions. However, in the sea lion ears, both the periotic and tympanic bones are firmly embedded in the skull, therefore the skull vibrations will certainly be carried to both the periotic and tympanic bones directly, and drive the ossicular chain, resulting in complex motions at the stapes footplate in the middle ear.

Previous studies have calculated TFs to predict audiograms for cetaceans (Tubelli et al., 2012; 2018; Cranford and Krysl, 2015). Here we calculated the frequency-dependant TF between the amplitude of the incident sound pressure wave and the magnitude of the velocity of the stapes footplate for the IA and UW models, as shown in Figure 9.

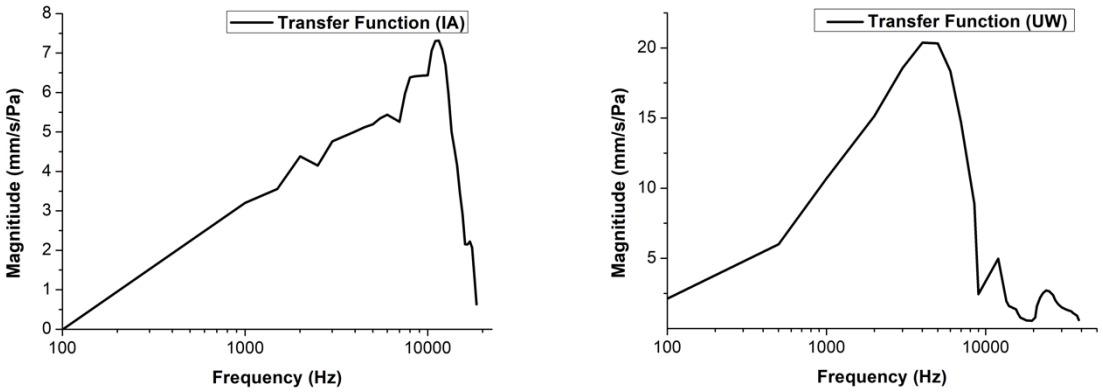

Figure 9. Transfer functions for the IA and UW models.

The curves of both TFs showed a similar trend but different peaks. The peak in the TF of the IA model was slightly above 10 kHz whereas the peak in the TF of the UW model was below 10 kHz. The TFs attenuated sharply at higher frequencies. Based on the two TFs, we attempted to predict the in-air and underwater audiograms for the ASL.

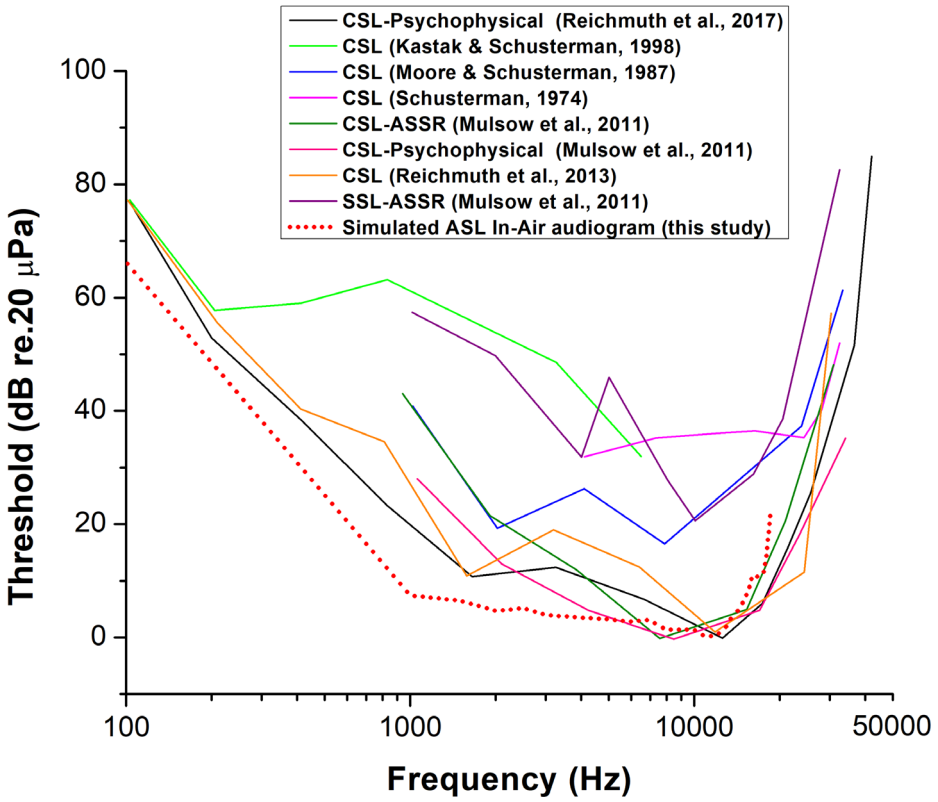

Figure 10. Predicted in-air audiogram of ASL. The simulated in-air audiogram was compared to the previously measured aerial hearing thresholds of several individual California sea lions (CSL) and Steller sea lions (SSL).

Neither the auditory capabilities nor the auditory thresholds have ever been measured for an ASL. Therefore, the audiogram curves can only be calibrated with respect to the minimum audible pressure values. In this research, we set the hearing thresholds to be similar to those previously measurement of a CSL, which has the minimum threshold at 0 dB re 20 µPa in air and 58 dB re 1µPa in water, respectively (Reichmuth et al., 2017; Kastelein et al., 2023). Then the minimum threshold pressure across all frequencies can be estimated and the threshold curve can be predicted from the TF; the results are shown in Figures 10 and 11.

For the in-air audiogram, the lowest predicted in-air threshold (~0 dB) for ASL was found at approximately 10.5 kHz with a gradual increase in thresholds at lower frequencies (on a log-f plot) and a steeper increase at higher frequencies (higher than 10.5 kHz). The region of best sensitivity (based on the lowest 40 dB range) was found at ~350 Hz to 20 kHz, which was close to most of the data measured for CSLs except the two curves obtained by Kastak & Schusterman (1998) and Schusterman (1974). The general shape of our curve was similar to both the CSL and Steller sea lions (SSL). Compared to the measured data of a SSL (the purple line in Figure 10), our predicted in-air audiogram curve showed a closer resemblance to the measured data of CSLs (Muslow et al., 2011; Reichmuth et al., 2013; Reichmuth et al., 2017), albeit somewhat our results showed that ASLs might have higher sensitive in the frequency range of 800 Hz–4 kHz than both the CSL and the SSL. Note that the SSL seemed to have less sensitivity across the entire frequency range compared to the CSL and the ASL.

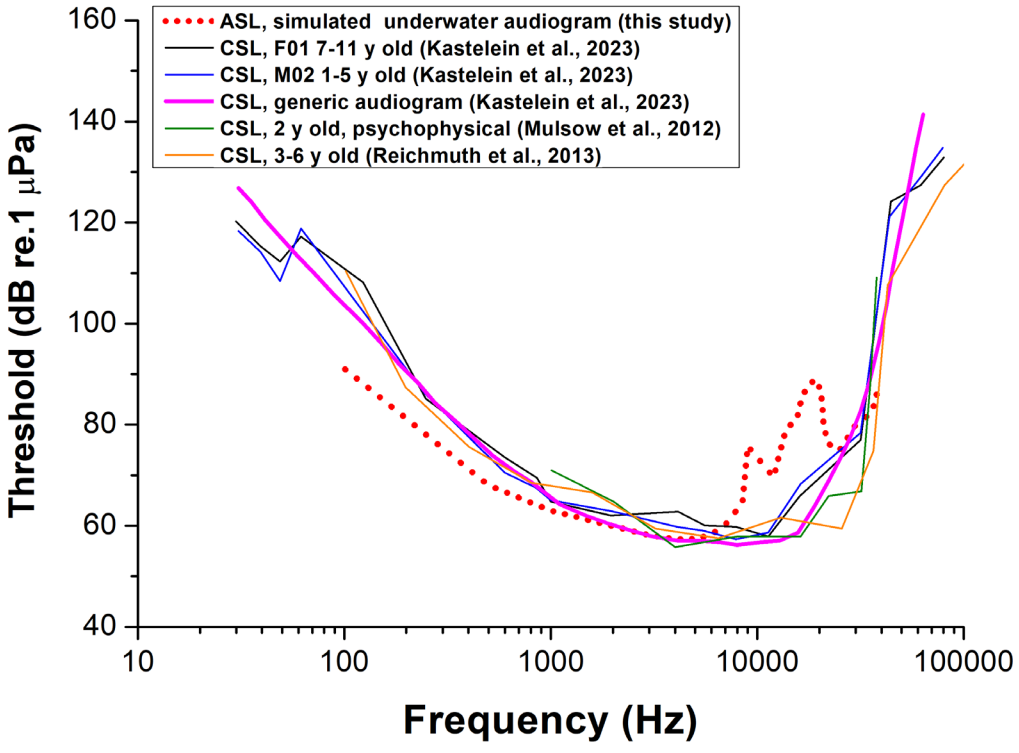

Figure 11. Predicted underwater audiogram of the ASL. The simulated underwater audiogram was compared to the previously measured underwater hearing thresholds of multiple CSL. The magenta curve shows the generic underwater audiogram.

For the underwater audiogram, the lowest predicted underwater threshold was at ~58 dB at approximately 5 kHz. The region of best hearing sensitivity was found at ~100 Hz to 40 kHz, the entire frequency range we simulated. Kastelein et al. (2023) calculated the generic audiogram for CSLs by

fitting an auditory weighting function (Southall et al., 2019) to the combined detection thresholds of this species based on the hearing thresholds measured from multiple CSLs (the magenta curve in Figure 11). The frequency-dependent patterns of sensitivity from our modelling results agreed well with the generic CSL audiogram, albeit our results suggested that ASLs might have slightly lower thresholds in the low-frequency range (100–800Hz) but higher thresholds in the frequency range of 9–20 kHz.

In general, our predicted audiograms, both in air and under water, were a good fit to those recently published hearing threshold data in terms of the form and range of auditory sensitivity.

5 Discussion

5.1 Predicted Audiograms

The hearing apparatus in mammals is a bandpass system. The middle ear component of the audiogram, represented by the TF, is a major contributor to the frequency response of the hearing threshold (Ruggero and Temchin, 2002). This likely reflects the audiogram peak sensitivities; the external and inner ears form additional components with each of the contributing important elements to the audiogram.

In comparison to previously published aerial audiograms, our predicted in-air audiogram did not align with the data tested by Schusterman (1974) and Kastak & Schusterman (1998) (Figure 10). It should be noted that the data measured by Schusterman (1974) and Kastak & Schusterman (1998) were also not in line with other CSL data in Figure 10. The discrepancy among the studies might be due to the testing condition. Instead of performing the testing in controlled conditions (e.g., acoustically controlled indoor enclosures), Schusterman (1974) tested a sea lion in the field and Kastak & Schusterman (1998) tested a sea lion in outdoor environments with headphones (both in less controlled conditions). This is likely the reason for obtaining curves with distinctly different shapes and significantly higher thresholds compared to other data. In contrast, the data from Reichmuth et al. (2013; 2017) were measured in the same indoor acoustic chamber, and the data from Moore & Schusterman (1987) and Mulsow et al. (2011) were measured in similar ad hoc noise-attenuating testing rooms. The similarity was visible in Figure 10, suggesting that the data measured in the same/similar controlled experiment condition were generally close. In addition, although the general shape of the SSL aerial audiogram was similar to those of the CSLs, the hearing thresholds were clearly higher across the entire frequency range, suggesting the hearing sensitivity varied among different sea lion species. This is likely related to the morphology differences between Families of Otariinae, such as the different head sizes, the anatomy differences of the head, etc. For the CSL, the male sea lion weighs on average 300 kg and is about 2.4 m long, while the female sea lion weighs 100 kg and is 1.8 m long. For the ASL, the male sea lion weighs on average 300 kg and grows to about 2.5 m long, while the female sea lion weighs approximately 105 kg and grows to a length of about 1.8 m. Both weight and size of CSL and ASL are close, suggesting that choosing tested audiograms of CSLs to convert our simulation results was reasonable. In contrast, the SSL is much larger than these two, which can weigh 1000 kg and grow to a length of 3 m. This distinct morphology difference could cause differences in the patterns of skull deformation and alter the sound reception process, resulting in different audiograms across the species. This is also the reason that it is critical to study hearing in ASLs if we aim to better understand and mitigate the negative effects of anthropogenic noise on this endangered species.

5.2 The Limitations of the Models and Future Work

Note that the audiograms we predicted in this study are approximations, some limitations need to be addressed and to be improved in the future.

Firstly, as we mentioned in the methods section (see 3.3 above), due to safety and health concerns, the tissue properties of the specimen were not measured in this research. Instead, we used the HU-to-density and HU-to-velocity relationships obtained from the previous study to convert the HU distribution of ASL head tissues. The methods were used to convert tissue properties for multiple odontocete species, such as a harbour porpoise (Wei et al., 2017; 2020), dead and live bottlenose dolphins (Wei et al., 2018a; 2020; 2023), and a Yangtze finless porpoise (Wei et al., 2018b). The FE models were constructed for each species based on the converted parameters. The outcomes of the FE models showed good agreement to direct measurements from the corresponding live, echolocating animals, proving the reliability of this method. Nevertheless, conducting vivo measurements to measure the tissue properties of the ASL tissues would still be an important future work as no such work has been documented before.

Secondly, our IA model only predicted the in-air audiogram from 100 Hz to 20 kHz and the UW model only predicted the underwater audiogram from 100 Hz to 40 kHz. 3D finite-element modelling requires massive computation costs, especially for the IA model. The sound speed of the air used in the model was 340 m/s, which was much lower than the sound speed of the sea water (1500 m/s), making the wavelength of the sound wave in the IA model much lower than the one in the UW model at the same frequencies. For the 3D acoustic modelling, the rule of thumb for meshing wave problems is to apply at least five to six second-order mesh elements per local wavelength in order to resolve waves. Therefore, the IA model ended up with 8.73 million DOFs at a maximum frequency of 20 kHz while the UW model ended up with 3.82 million DOFs at a maximum frequency of 40 kHz. After multiple tests, we found that our workstation for this research, which has a 384 GB RAM, can only efficiently calculate the model with DOFs of no more than 9 million.

Thirdly, the ossicular chain of the ASL is very small, with a size of less than 5 mm in our study. The thickness of the XCT data was 0.8 mm (the resolution of the XCT), meaning that only several slices can be used to reconstruct the ossicular chain. The automatic segmentation function in the software cannot provide accurate geometry information for ossicular chain reconstruction. Therefore, we had to manually perform segmentation slice by slice based on the sea lion anatomy knowledge. Therefore, only a general shape of the ossicular chain can be reconstructed. Performing microCT scanning on the ear (requires the removal of the ear from the head) would be important future work to reconstruct a much more detailed ear structure, especially the ossicular chain.

Fourthly, the anatomical configuration of the individual varies with age and sex, causing slight differences when sound interacts with the animal structures. Additionally, health and prior sound exposure might affect neural processes and hence individual hearing sensitivity. Thus, audiograms among the individuals of the same species differ somewhat. For example, the variation of the measured underwater audiograms among the CSLs of different ages can be clearly seen in Figure 10. Therefore, collecting more ASL specimens for modelling is an important future work to capture variability in audiograms of this endangered species.

Finally, early work on using FEA to estimate hearing thresholds on baleen whales have shown that different locations of source excitation could cause reasonably different response curves (Tubelli et al., 2012; 2018). Therefore, it would be important to test this theory on both IA and UW models in the future.

5.3 Potential Effects of Anthropogenic Noise on Endangered ASLs

The modelling results indicate that ASLs are sensitive at frequencies emitted by common anthropogenic noise sources. In air, traffic noise from cars and aircraft, and construction noises will be audible to ASLs (see Schoeman et al. 2022 for an overview of in-air noise spectra). Under water, ship traffic is a primary source of noise between 20 and 1000 Hz (Urick, 1983). Pile driving is common in coastal regions, emitting broadband acoustic energy between 50 Hz and 5 kHz (e.g., Erbe 2009).

Another common noise source in the ocean is the airgun signals from seismic surveys, with most acoustic energy below 500 Hz (e.g., Erbe and King, 2009). Military sonar typically ranges between 1 and 10 kHz (Nowacek et al., 2007). It appears that ASLs can hear these sounds well under water. The potential effects of these noise sources on ASLs range from behavioural disturbance to acoustic masking (i.e., interference with acoustic signalling and listening by sea lions), stress, and hearing loss (e.g., Erbe et al., 2018; 2019).

The potential effects of in-air and underwater noise on ASLs, and the ranges over which they occur, may now be estimated. To estimate the ranges over which noise sources are audible, the source spectrum (see source spectra determined in Project 7.1) needs to be found and integrated into critical bands, and acoustic propagation loss at critical band centre frequencies needs to be applied (see sound propagation modelling in Project 7.1), to yield received critical band levels as a function of range. These may then be compared to the ambient noise spectra (as monitored in Project 7.1; also integrated into critical bands) and to the audiogram. At any ranges and critical band frequencies at which the received level exceeds both the ambient noise level and the audiogram, the noise source is deemed audible (see examples in Erbe et al., 2016; 2022). The ranges over which anthropogenic noise may mask signals important to sea lions may be modelled in a similar way. To estimate over which ranges hearing loss may be incurred, the thresholds from Southall et al. (2019) may be applied.

6 Conclusions/Recommendations

This is the first study using CT imaging-based finite-element modelling techniques to predict auditory sensitivity for the endangered ASL both in air and under water. It is the only currently available method capable of predicting audiograms for ASLs across a broad spectrum of sound frequencies, between 100 Hz and 20 kHz in air and 100 Hz and 40 kHz underwater. The results provide a valuable indication of the ranges of frequencies and levels that can be heard by this endangered species. The predicted audiograms are generally similar to those previously published for CSLs, which have a similar size to the ASL. The results suggested that the guidance of Southall et al. (2019) for CSLs can be applied as a reference in the EIA and management plans, for instance, distances for management (exclusion and observation) zones. The audiograms from this study provide important information that can also be used to predict the effects of anthropogenic underwater noise and to assess the extent to which biologically relevant sounds are masked by anthropogenic noise. The study develops important tools to study the sound reception process and predict auditory sensitivity for inaccessible animals if an animal species shares a similar sound reception mechanism. Finally, this study provides valuable data for marine fauna conservation and management. The outputs from this study can assist efforts in understanding the potential impacts, designing noise reduction methods, and devising mitigation plans for ASLs.

7 References

Aarts G, Brasseur S, Kirkwood R (2018). Behavioural response of grey seals to pile-driving. (Wageningen Marine Research report; No. C006/18). Wageningen Marine Research.

Ahonen H, Stow AJ, Harcourt RG, Charrier I (2014). Adult male Australian sea lion barking calls reveal clear geographical variations. Anim Behav 97: 229–239.

Aroyan JL (2001) Three-dimensional modeling of hearing in *Delphinus delphis*. J Acoust Soc Am 110(6): 3305–3318.

Au WWL (1993). The sonar of dolphins. Springer-Verlag.

Azhari H (2010) Appendix A: Typical Acoustic Properties of Tissues. In: Basics of Biomedical Ultrasound for Engineers. IEEE, pp. 313–314.

Bayne, EM, Bayne EM, Habib L, Boutin S (2008) Impacts of chronic anthropogenic noise from energy-sector activity on abundance of songbirds in the boreal forest. Conserv Biol 22: 1186–1193.

Bérenger JP (1994) A perfectly matched layer for the absorption of electromagnetic waves. J Comput Phys 114(2): 185–200.

Brittan-Powell EF, Dooling RJ, Gleich O (2002) Auditory brainstem responses in adult budgerigars (*Melopsittacus undulatus*). J Acoust Soc Am 112: 999−1008.

Brittan-Powell EF, Dooling RJ, Ryals B, Gleich O (2010) Electrophysiological and morphological development of the inner ear in Belgian Waterslager canaries. Hear Res 269: 56−69.

Buhler P (1992) Light bones in birds. LA Mus Nat Hist Sci Ser 36: 385–394.

Campbell RA, Holley D, Christianopoulos D, Caputi N, Gales, N (2008) Mitigation of incidental mortality of Australian sea lions in the west coast rock lobster fishery. Endanger Species Res 5: 345–358.

Clark CW (1990) Acoustic behavior of mysticete whales. In: Thomas JA, Kastelein RA (eds), Sensory Abilities of Cetaceans: Laboratory and Field Evidence. New York: Plenum Publishing Corporation. pp. 571–583.

Cranford TW, Krysl P (2015) Fin whale sound reception mechanisms: Skull vibration enables low-frequency hearing. PLoS ONE 10(1): Article e0116222.

Currey JD (1979). Mechanical properties of bone tissues with greatly differing functions. J Biomech 12: 313–319.

DeAngelo KM (2008) Assessing hearing loss due to ototoxic drugs in the zebra finch. Master dissertation, University of Maryland, College Park.

De Greef D, Pires F, Dirckx JJ (2017) Effects of model definitions and parameter values in finite element modeling of human middle ear mechanics. Hear Res 344: 195–206.

DCCEEW (2013) Recovery Plan for the Australian Sea Lion (Neophoca cinerea). www.dcceew.gov.au/environment/biodiversity/threatened/recovery-plans/recovery-plan-australian-sea-lion-neophoca-cinerea-2013

Duck FA (1990) Physical Properties of Tissue: A Comprehensive Reference Book (Academic Press, San Diego, CA).

Dumont ER (2010) Bone density and the lightweight skeletons of birds. Proc R Soc B 2772193–2198.

Erbe C (2009) Underwater noise from pile driving in Moreton Bay, Qld. Acoust Aust 37 (3): 87–92.

Erbe C, Duncan A, Vigness-Raposa KJ (2022) Introduction to sound propagation under water. In: Erbe C, Thomas JA (eds) Exploring Animal Behavior Through Sound: Volume 1: Methods. Springer International Publishing, Cham, pp. 185–216.

Erbe C, Dunlop R, Dolman S (2018) Effects of Noise on Marine Mammals. In: Slabbekoorn H, Dooling RJ, Popper AN, Fay RR (eds) Effects of Anthropogenic Noise on Animals. Springer New York, New York, NY, pp. 277–309.

Erbe C, King AR (2009) Modelling cumulative sound exposure around marine seismic surveys. J Acoust Soc Am 125 (4): 2443–2451.

Erbe C, Marley S, Schoeman R, Smith JN, Trigg L, Embling CB (2019) The effects of ship noise on marine mammals--A review. Front Mar Sci 6: 606.

Erbe C, Reichmuth C, Cunningham KC, Lucke K, Dooling RJ (2016) Communication masking in marine mammals: A review and research strategy. Mar Pollut Bull 103: 15–38.
Frahnert S, Lindner M, Bendel E, Frahnert, KH, Westphal, N, Dahne M (2019) 3D-Visualization of the Ear Morphology of Penguins (*Spheniscidae*): Implications for Hearing Abilities in Air and Underwater. Proc Mtgs Acoust 37: 010018.
Francis CD, Kleist NJ, Davidson BJ, Ortega CP, Cruz A (2012) Behavioral responses by two songbirds to natural-gas-well compressor noise. Ornithol Monogr 74(1): 36–46.
Gales NJ, Cheal AJ, Pobar GJ, Williamson P (1992) Breeding biology and movements of Australian sea lions, *Neophoca cinerea*, off the west coast of Western Australia. Wildl Res 19(4): 405–415.
Gales NJ, Shaughnessy PD, Dennis TE (1994) Distribution, abundance and breeding cycle of the Australian sea lion Neophoca cinerea (*Mammalia: Pinnipedia*). J Zool 234: 353–370.
Gan RZ, Feng B, Sun Q (2004) Three-dimensional finite element modeling of human ear for sound transmission. Ann Biomed Eng 32(6): 847–859.
Goerlitz HR, Greif S, Siemers BM (2008) Cues for acoustic detection of prey: insect rustling sounds and the influence of walking substrate. J Exp Biol 211: 2799–2806.
Gordon J, Gillespie D, Potter J, Frantzis A, Simmonds MP, Swift R, Thompson D (2003) A review of the effects of seismic surveys on marine mammals. MTSJ 37: 16–34.
Goldsworthy SD (2015) *Neophoca Cinerea*. The IUCN Red List of Threatened Species 2015.
Gwilliam J, Charrier I, Harcourt RG (2008) Vocal identity and species recognition in male Australian sea lions, *Neophoca cinerea*. J Exp Biol 211(14): 2288–95.
Homma K, Du Y, Shimizu Y, Puria S (2009) Ossicular resonance modes of the human middle ear for bone and air conduction. J Acoust Soc Am 125(2): 968–979.
Homma K, Shimizu Y, Kim N, Du Y, Puria S (2010) Effects of ear-canal pressurization on middle-ear bone- and air-conduction responses. Hear Res 263(1): 204–215.
Ihlenburg F (2006) Finite element analysis of acoustic scattering (Springer Science, Business Media).
Kastak D, Schusterman RJ (1998) Low-frequency amphibious hearing in pinnipeds: Methods, measurements, noise, and ecology. J Acoust Soc Am 103: 2216–2228.
Kastelein RA, Helder-Hoek L, Acoleyen LV, Defillet LN, Huijser LAE, Terhune JM (2023) Underwater Sound Detection Thresholds (0.031–80 kHz) of Two California Sea Lions (*Zalophus californianus*) and a Revised Generic Audiogram for the Species. Aquat Mamm 49(5): 422–435.
Kastelein RA, van Schie R., Verboom WC, de Haan D (2005) Underwater hearing sensitivity of a male and a female Steller sea lion (*Eumetopias jubatus*). J Acoust Soc Am 118: 1820–1829.
Ketten DR (1994) Functional analysis of whale ears: adaptations for underwater hearing. IEEE Proc Underwater Acoust 1: 264–270.
Ketten DR (1997) Structure and function in whale ears. Bioacoustics 8: 103–135.
Ketten DR (2000) Cetacean ears. In: Au WWL, Popper AN, Fay RR (eds), Hearing by whales and dolphins. New York: Springer-Verlag. pp. 43–108.
Koike T, Wada H, Kobayashi T (2002) Modeling of the human middle ear using the finite-element method. J Acoust Soc Am 111(3): 1306–1317.
Krysl P, Hawkins AD, Schilt C, Cranford TW (2012) Angular oscillation of solid scatterers in response to progressive planar acoustic waves: do fish otoliths rock? PLoS ONE 7: e42591.
Lohr B, Brittan-Powell EF, Dooling RJ (2013) Auditory brainstem responses and auditory thresholds in woodpeckers. J Acoust Soc Am 133: 337−342.
Matthews JN, Rendall LE, Gordon JCD, Macdonald DW(1999) A review of frequency and time parameters of cetacean tonal calls. Bioacoustics 10: 47–71.
Moore PWB, Schusterman RJ (1987) Audiometric assessment of northern fur seals, *Callorhinus ursinus*. Mar Mammal Sci 3: 31–53.
Mulsow J, Finneran JJ, Houser DS (2011) California sea lion (*Zalophus californianus*) aerial hearing sensitivity measured using auditory steady-state response and psychophysical methods. J Acoust Soc Am 129: 2298–2306.
Mulsow J, Houser DS, Finneran JJ (2012) Underwater psychophysical audiogram of a young male California sea lion (*Zalophus californianus*). J Acoust Soc Am 131: 4182–4187.

Mulsow JL, Reichmuth C (2010) Psychophysical and electrophysiological aerial audiograms of a Steller sea lion (*Eumetopias jubatus*). J Acoust Soc Am 127: 2692–2701.

Mulsow J, Reichmuth C, Gulland FMD, Rosen DAS, Finneran JJ (2011) Aerial audiograms of several California sea lions (*Zalophus californianus*) and Steller sea lions (*Eumetopias jubatus*) measured using single and multiple simultaneous auditory steady-state response methods. J Exp Biol 214: 1138–1147.

Nowacek DP, Thorne LH, Johnston DW, Tyack PL (2007) Responses of cetaceans to anthropogenic noise. Mammal Rev 37(2): 81–115.

Ortega, CP (2012) Effects of noise pollution on birds: A brief review of our knowledge. Ornithol Monogr 74: 6–22.

Reichmuth C, Holt MM, Mulsow J, Sills JM, Southall BL (2013) Comparative assessment of amphibious hearing in pinnipeds. J Comp Physiol A Neuroethol Sensory Neural Behav Physiol 199: 491–507.

Reichmuth C, Sills JM, Ghoul A (2017) Psychophysical audiogram of a California sea lion listening for airborne tonal sounds in an acoustic chamber. Proc Meet Acoust 30: 010001.

Reichmuth C, Southall BL (2012) Underwater hearing in California sea lions (*Zalophus californianus*): Expansion and interpretation of existing data. Mar Mammal Sci 28: 358–363.

Ruggero MA, Temchin AN (2002) The roles of the external, middle, and inner ears in determining the bandwidth of hearing. PNAS 99: 13206–13210.

Sadé J, Handrich Y, Bernheim J, Cohen D (2008) Pressure equilibration in the penguin middle ear. Acta Otolaryngol 128(1): 18–21.

Schusterman RJ (1974) Auditory sensitivity of a California sea lion to airborne sound. J Acoust Soc Am 56: 1248–1251.

Schusterman RJ, Balliet RF, Nixon J (1972) Underwater audiogram of the California sea lion by the conditioned vocalization technique. J Exp Anal Behav 17: 339–350.

Schoeman RP, Erbe C, Pavan G, Righini R, Thomas JA (2022) Analysis of soundscapes as an ecological tool. In: Erbe C, Thomas JA (eds) Exploring Animal Behavior Through Sound: Volume 1: Methods. Springer International Publishing, Cham, pp. 217–267.

Slabbekoorn H, Dooling RJ, Popper AN, Fay RR (2018) Effects of Anthropogenic Noise on Animals. Springer Verlag, New York.

Salas AK, Wilson PS, Fuiman LA (2019a) Predicting pressure sensitivity through ontogeny in larval red drum (*Sciaenops ocellatus*). Proc Mtgs Acoust 37: 010006.

Salas AK, Wilson PS, Fuiman LA. (2019b). Ontogenetic change in predicted acoustic pressure sensitivity in larval red drum (*Sciaenops ocellatus*). J Exp Biol 222: jeb201962.

Soldevilla MS, McKenna MF, Wiggins SM, Shadwick RE, Cranford TW, Hildebrand JA (2005) Cuvier's beaked whale (*Ziphius cavirostris*) head tissues: Physical properties and CT imaging. J Exp Biol 209: 2319–2332.

Southall BL, Bowles A, Ellison W, Finneran J, Gentry R, Greene CJr, Kastak D, Ketten D, Miller J, Nachtigall P, Richardson W, Thomas J, Tyack P (2008) Marine mammal noise exposure criteria: initial scientific recommendations. Bioacoustics 17: 273–275.

Southall BL, Finneran JJ, Reichmuth C, Nachtigall PE, Ketten DR, Bowles AE, Ellison WT, Nowacek DP, Tyack PL (2019) Marine mammal noise exposure criteria: Updated scientific recommendations for residual hearing effects. Aquat Mamm 45 (2):125–232.

Thompson D, Sjoberg M, Bryant ME, Lovell, P, Bjorge, A (1998) Behavioral and physiological responses of harbour (*Phoca vitulina*) and grey (*Halichoerus grypus*) seals to seismic surveys. Report to the European Commission of BROMMAD Project MAS2 C7940098.

Thompson LL, and Pinsky PM (1994) Complex wave number Fourier analysis of the p-version finite element method. Comput Mech 13: 255–275.

Tubelli AA, Zosuls A, Ketten DR, Mountain DC (2018) A model and experimental approach to the middle ear transfer function related to hearing in the humpback whale (*Megaptera novaeangliae*). J Acoust Soc Am 144(2): 525–535.

Tubelli AA, Zosuls A, Ketten DR, Mountain DC (2014) Elastic modulus of cetacean auditory ossicles. Anatom Rec 297(5): 892–900.

Tubelli AA, Zosuls A, Ketten DR, Yamato M, Mountain DC (2012) A prediction of the minke whale (*Balaenoptera acutorostrata*) middle-ear transfer function. J Acoust Soc Am 132(5): 3263–3272.

Urick RJ (1983) Principles of Underwater Sound. McGraw-Hill, New York, pp. 1–423.

Wang X, Gan RZ (2016) 3D finite element model of the chinchilla ear for characterizing middle ear functions. Biomech Model Mechanobiol 15(5): 1263–1277.

Wei C, Au WWL, Ketten DR (2020) Modeling of the near to far acoustic fields of an echolocating bottlenose dolphin and harbor porpoise. J Acoust Soc Am 147(3): 1790–1801.

Wei C, Au WWL, Ketten DR, Song Z, Zhang Y (2017) Biosonar signal propagation in the harbor porpoise's (*Phocoena phocoena*) head: the role of various structures in the formation of the vertical beam. J Acoust Soc Am 141(6): 4179–4187

Wei C, McCauley RD (2022) Numerical modeling of the impacts of acoustic stimulus on fish otoliths from two directions. J Acoust Soc Am 152(6): 3226–3234.

Wei C, Au WWL, Ketten DR, Zhang Y (2018a) Finite element simulation of broadband biosonar signal propagation in the near- and far-field of an echolocating Atlantic bottlenose dolphin (*Tursiops truncatus*). J Acoust Soc Am 143(5): 2611–2620.

Wei C, Song Z, Au WWL, Zhang Y, Wang D (2018b) A numerical evidence of biosonar beam formation of a neonate Yangtze finless porpoise (*Neophocaena asiaeorientalis*). J Theor Comput Acoust, 26(2): 1850009: 1–15.

Wei C, Houser D, Erbe C, Matrai E, Ketten DR, Finneran, J, Does rotation increase the acoustic field of view? Comparative models based on CT data of a live dolphin versus a dead dolphin. Bioinspir Biomim Biomim 18–0035006.

Wei C, Wang Z, Song Z, Wang K, Wang D, Au WWL, Yu Z (2015) Acoustic property reconstruction of a neonate Yangtze finless porpoise's (*Neophocaena asiaeorientalis*) head based on CT Imaging. PLoS ONE 10: e0121442.

Submitted as draft	19/03/2024
Reviewed completed	18/04/2024
Submitted as revised draft	20/05/2024
Approved by Science Program Leadership Team	24/05/2024
Approved by WAMSI CEO	26/06/2024
Final report	

WESTERN AUSTRALIAN
MARINE SCIENCE
INSTITUTION